RSC Advances



View Article Online

View Journal | View Issue

PAPER



Cite this: RSC Adv., 2016, 6, 77083

Received 30th May 2016 Accepted 27th July 2016 DOI: 10.1039/c6ra13993k

www.rsc.org/advances

Introduction

Cancer has become one of the greatest threats to human health worldwide.^{1,2} However, the current clinical cancer treatment methods, including surgery, radiotherapy and chemotherapy, are limited by their serious side effects such as risks of toxicity to normal cells and damage of the immune system.^{3,4} Therefore, developing new therapies and minimizing harm to normal cells is extremely urgent to fight against this fatal disease. In this regard, photothermal therapy (PTT), owing to its high selectivity, minimal invasive approach, therapeutic effect and low number of side effects, could be developed as an alternative cancer treatment method.^{5,6} The mechanism of PTT involves "burning" of malignant cells by employing heat generated by photothermal agents from light absorption. Recently, several nanomaterials and organic dyes have been explored as PTT

Facile exfoliation of MoS₂ nanosheets by protein as a photothermal-triggered drug delivery system for

Rui Deng,‡^a Hai Yi,‡^a Fangyi Fan,^a Li Fu,^a Yan Zeng,^a Yi Wang,^a Yecheng Li,^a Yilan Liu,^a Shengjun Ji^b and Yi Su^{*a}

synergistic tumor therapy[†]

We report here a facile method to prepare molybdenum disulfide (MoS₂) nanosheets using protein, with high near-infrared (NIR) absorbance and high-efficiency drug loading ratio, as a photothermal-triggered drug delivery system for synergistic tumor therapy. MoS₂ nanosheets were prepared by physical ultrasonic exfoliation in the presence of bovine serum albumin (BSA), which not only acted as an auxiliary agent of ultrasonic exfoliation, but also functioned as a surfactant for MoS₂ nanosheets. The resulting MoS₂ nanosheets exhibited great stability and a high surface-area-to-mass that had a loading ratio of about 180% (w/w) of the anti-cancer drug, resveratrol (RV). Exposing MoS₂ nanosheets in Raji cells for 3 h resulted in a 58.2% cellular uptake ratio and low cytotoxicity for an extra 21 h incubation. After loading RV onto MoS₂ nanosheets (MoS₂–RV), RV molecules could be released from the MoS₂ surface, triggered by NIR laser irradiation (1 W cm⁻²), thus enhancing the cell viability inhibition effect. MoS₂–RV at 24 h post-injection into tumor-bearing mice could passively target and accumulate to the tumor region and, along with NIR laser irradiation for 5 min, the tumor was efficiently ablated and exhibited no relapse. These results, including *in vitro* and *in vivo* tumor therapy studies, demonstrated an excellent synergistic tumor therapeutic effect of the NIR-controlled RV delivery and release system of MoS₂–RV, in comparison with chemotherapy and photothermal therapy (PTT) alone.

agents, for example, metal nanoparticles^{7–10} based on Cu–, Au–, Ag– and Pd– and organic dyes.^{11,12} Despite exhibiting an efficient photothermal effect, metallic nanoparticles have low loading capacity of functional molecules due to a low surfacearea-to-mass ratio. Organic dyes such as indocyanine green (ICG), which is approved by the FDA, has a very small size, high photothermal conversion efficiency and low cytotoxicity; however, the short half-life and instability under intense laser irradiation limit its PTT applications.^{13,14} Currently, twodimensional (2D) layered transition metal dichalcogenide (TMDC) nanosheets have drawn attention due to their novel physico-chemical properties such as high surface-area-to-mass ratio, near-infrared (NIR) absorbance, and their ease of modification, *etc.*¹⁵

Molybdenum disulfide (MoS₂) is a type of TMDC nanosheet where the MoS₂ sheets are bound to each other by weak van der Waals forces.^{16,17} After exfoliation to thin and ultra-small particles, the NIR absorbance increases significantly compared with their bulk forms due to the quantum confinement effect,^{18,19} thus making MoS₂ nanosheets a promising candidate to be a photothermal agent. Wang and co-workers have prepared MoS₂ nanosheets after polyethylene glycol modification and soybean phospholipid encapsulation, respectively, for efficient cancer photothermal therapy (PTT).²⁰⁻²² However, single traditional PTT may not suppress tumor growth completely, thus

^aHematology Department and Hematopoietic Stem Cell Transplantation and Cell Immunotherapy Center, Cheng Du Military General Hospital of PLA, Cheng Du, Sichuan 610083, China. E-mail: yisu0109@sina.com; Tel: +86-028-86570701

^bUrology Department, Cheng Du Military General Hospital of PLA, Cheng Du, Sichuan 610083, China

[†] Electronic supplementary information (ESI) available. See DOI: 10.1039/c6ra13993k

[‡] These authors contributed equally to this paper.

generating a tumor relapse for long-term tumor therapy.^{23,24} Therefore, a more efficient tumor therapy strategy—simultaneous delivery of heat and drug into the tumor region—may overcome the shortcoming of the traditional single tumor PTT and chemotherapy. Due to the graphene-like atomically-thin 2D structure of MoS₂ nanosheets that showed a large surface-areato-mass ratio, it enabled highly efficient drug loading of MoS₂ nanosheets for cancer therapy. Liu and co-workers stabilized MoS₂ nanosheets by using polyethylene glycol (PEG) to load doxorubicin (DOX) for combined PTT and chemotherapy of cancer.²⁵ MoS₂ has also been reported as a NIR photothermal delivery system that triggers DOX release for enhanced tumor therapy.^{23,26}

In this study, we prepared MoS₂ nanosheets employing a facile method using bovine serum albumin (BSA) in aqueous solution under ultrasonication. MoS2 nanosheets exhibited great biocompatibility, high NIR absorbance and photothermal effect. Resveratrol (RV), a natural non-water-soluble antioxidant extracted from Polygonum cuspidatum was reported that can reduce blood viscosity, inhibit platelet aggregation and vasodilation, and prevent the occurrence and development of cancer.27,28 RV was loaded onto the MoS2 surface (MoS2-RV) to enhance water solubility. Moreover, we found that the MoS₂ nanosheets could deliver both heat and drugs to the tumor region simultaneously. At the same time, this system (MoS₂-RV) also exhibited a synergistic cancer therapeutic effect and minimal side effects associated with NIR-mediated hyperthermia and photothermal-triggered local drug release, which were demonstrated both in vitro and in vivo.

Experimental section

Materials

 MoS_2 (powder, 99%) was purchased from Sigma-Aldrich. RPMI-1640 medium and fetal bovine serum (FBS) were purchased from Gibco. 4',6'-Diamidino-2-phenylindole (DAPI) was purchased from Invitrogen (Carlsbad, CA, USA). Bovine serum albumin (BSA, \geq 98.0%) was purchased from Biosharp Co. LTD. Cell Counting Kit-8 (CCK-8) was procured from Dojin Chemical Laboratory Co., Ltd.

Preparation of MoS₂ nanosheets

MoS₂ nanosheets were prepared following a previously reported method.¹⁹ In brief, 20 mg of MoS₂ powder and 50 mL of water were added into a 100 mL glass bottle and stirred for 10 min. The aqueous dispersion of MoS₂ powder was firstly sonicated in an ice-bath by using tip sonication (Xi'an Tai Kang, China, 650 W, 20 kHz) with 90% amplitude for 2 h, and then 20 mg of BSA powder was added into the mixture followed by sonication using a sonic ice-bath with a low energy density (CQ-2000BD, ShanghaiYuejin, China) for 10 h. The resulting hybrid was centrifuged at 8000 rpm for 20 min to remove large aggregates. The supernatant was collected and purified by further centrifugation at 16 000 rpm for 30 min and stored at 4 °C.

RV was loaded onto MoS_2 nanosheets by adding various concentration of RV (dissolved in DMSO) into a 10 mL MoS_2 water suspension (0.25 mg mL⁻¹) with constant stirring at room temperature for 24 h. Unbound RV was repeatedly filtered through a 30 kDa filter (Millipore) and centrifuged at 8000 rpm. The resulting MoS_2 -RV solution was stored at 4 °C. The amount of unbound RV was detected using a UV-vis spectrophotometer (Perkin-Elmer, USA) by monitoring the absorption peak of RV at 306 nm. All supernatants were collected. RV loading ratio was calculated using the following equation:

RV loading ratio(%) =
$$\frac{a-b}{c} \times 100\%$$

where a (mg) and b (mg) are the initial and unbound RV, respectively; c (mg) is the mass of MoS₂ nanosheets.

Characterizations

UV-vis absorption spectra were recorded using a UV-vis spectrophotometer (UV7502, Shanghai advanced photoelectric technology co., LTD, Shanghai, China). Atomic force microscopy (AFM) images were captured using a FM-Nanoview 6600 AFM. Transmission electron microscopy (TEM) images were collected on a Zeiss LIBRA 120 TEM. Dynamic light scattering (DLS) analysis was performed using a Zetasizer Nano ZS (Malvern Instruments). Optical photographs were taken with a Nikon D3200 digital camera. Thermogravimetric analysis (TGA) was performed using a TGA analyzer (Perkin Elmer Pyris 1, USA) under a constant heating rate of 10 °C min⁻¹ and continuous nitrogen flow. The intracellular fluorescence was observed using a commercial laser scanning microscope (LSM 510 system, Zeiss, Germany). The cell uptake ratio of the sample was analyzed by Flow cytometry (FCM, FACSCalibur, BD, New Jersey, USA). The Mo element mass of the nanocomposite was measured by using an inductively coupled plasma optical emission spectrometer (ICP-OES, ICAP 7000, Thermo Scientific, USA).

Photothermal effect

Water, 20 μ g mL⁻¹ bulk MoS₂ and MoS₂ nanosheets were continuously irradiated by 808 nm NIR laser (1 W cm⁻²) for 5 min. Temperature was detected by a thermocouple thermometer (HH802U, OMEGA, USA) every 30 seconds.

Cell line and cell culture

The human Burkitt's lymphoma cell line Raji cell came from American Type Culture Collection (ATCC) and was maintained in RPMI-1640 medium supplemented with 10% FBS, 1% penicillin and streptomycin solution at 37 °C in an atmosphere of 5% CO₂. In addition, the mouse bone marrow cells were isolated according to the protocol reported in the literature.²⁹ Briefly, 6–8 week old healthy Balb/c mice were euthanized and disinfected with 75% ethanol. The bones were taken out and placed in a Petri dish containing ice-cold RPMI-1640 media supplemented with 10% FBS and 1% penicillin and

Paper

streptomycin. After cutting off the epiphyses of the bones, a syringe filled with RPMI-1640 media supplemented with 10% FBS and 2 mM EDTA was used to flush the bone marrow cells from both ends of the bone. The obtained bone marrow cell suspensions were filtered through a 100 μ m filter. In addition, the red blood cells in the suspensions were lysed by resuspending the cell pellet in 0.2% NaCl for ~20 second followed by addition of a 1.6% NaCl solution. Centrifugation of 1500 rpm for 5 min at 4 °C was conducted to collect the bone marrow cells, which were then washed by RPMI-1640 media supplemented with 10% FBS and 2 mM EDTA three times. The collected bone marrow cells were cultured in an incubator at 37 °C in an atmosphere of 5% CO₂, and must be used within three days.

Cell uptake assay

To observe the cellular uptake, fluorescein isothiocyanate (FITC) was used to label MoS₂ nanosheets. Briefly, the MoS₂ water suspension (0.2 mg mL^{-1}) was simply mixed with 0.1 mLof FITC (2 mg mL $^{-1}$, dissolved in DMSO), followed by stirring at room temperature for 24 h. The resulting mixture was repeatedly filtered through a 30 kDa filter to remove the unbound FITC and washed by PBS thrice. The purified FITC labeled MoS₂ (MoS₂/FITC) was re-dispersed in distilled water. Raji cells adhered to glass slides in six-well plates and were incubated with free FITC or MoS₂/FITC at the same concentration of FITC $(0.05 \text{ mg mL}^{-1})$ for 4 h. The cells were washed with PBS thrice and then fixed by 0.2 mL of glutaraldehyde, followed by staining with DAPI for 10 min. The fluorescence images of cells were captured using the laser scanning microscope. In addition, the uptake ratios of MoS₂/FITC by Raji cells were analyzed using FCM through measuring FITC fluorescence. Ten thousands cells were recorded for each FCM analysis. The FITC fluorescence was excited using a 488 nm laser.

In vitro tumor therapy

Raji cells (5×10^4 cells per well) were seeded into 96-well plates in RPMI-1640 media and cultured for 24 h. Next, the media were replaced by fresh media containing MoS₂ nanosheets (25 µg mL⁻¹, 50 µg mL⁻¹, 100 µg mL⁻¹, and 200 µg mL⁻¹), RV, and MoS₂–RV (10 µg mL⁻¹, 20 µg mL⁻¹, 30 µg mL⁻¹, and 40 µg mL⁻¹ of RV). After incubating for an extra 24 h, the old media were discarded and the cells were washed by PBS three times mildly. A 100 µL CCK-8 working solution (10% CCK-8 + 90% RPMI-1640) was then added to each well, followed by incubation at 37 °C for 2 h. The absorbance value at 450 nm was detected using a microplate reader (Infinite 200 Pro, Tecan, Austria). The relative cell viability was calculated as an equation:

Relative cell viability (%) = $(A - A_0) \div (A_1 - A_0) \times 100\%$

where A was the absorbance of various sample-treated cells mixed with the CCK-8 working solution, A_0 was the absorbance of cells in media, and A_1 was the absorbance of cells mixed with the CCK-8 working solution. The experiment was carried out in triplicate. For *in vitro* PTT, Raji cells (5×10^4 cells per well) were seeded into 96-well plates in RPMI-1640 media and cultured for 24 h. The media were replaced by fresh media containing MoS_2 nanosheets, RV and MoS_2 -RV with the concentration as mentioned above. After incubating for 4 h, the cells were exposed under the 808 nm laser (1 W cm^{-2}) for 5 min, and then were incubated again for an extra 24 h. After this treatment, the CCK-8 assay was used to evaluate cell viabilities according to the procedures mentioned above.

Blood analysis

The Balb/c mice were injected with MoS_2 and MoS_2 -RV at MoS_2 doses of 15 mg kg⁻¹ (n = 6). Saline was used as the control. Animals were euthanized 7 and 21 days post-injection and whole blood was collected from each mouse *via* orbit for blood analysis. Blood analyses were conducted in the Hematology Department and Hematopoietic Stem Cell Transplantation and Cell Immunotherapy Center of Cheng Du Military General Hospital of PLA.

In vivo biodistribution and anticancer efficacy

All animal experiments were carried out under protocols approved by the Institutional Animal Care. To generate the tumor model, 100 μ L of PBS containing 1 × 10⁷ Raji cells were subcutaneously injected into the back of each Balb/c nude mice. After the tumor volume reached ~100 mm³, the mice were used for subsequent experiments. The tumor volume was calculated according to the following formula: *V* = length × width²/2.

To analyze the systemic biodistribution of MoS_2 -RV, the tumor-bearing nude mice were euthanized at 3 h, 1 day, 3 days, and 7 days post tail intravenous injection with MoS_2 -RV (150 μ L, [Mo] = 1 mg mL⁻¹). Major organs (heart, liver, spleen, lung, kidney, and tumor) were first weighed and then digested by aqua regia solution for 12 h. The uptake amounts of Mo elements in different tissues were quantified by ICP-OES.

For *in vivo* anticancer efficacy, the tumor-bearing nude mice were randomly divided into six groups (seven mice per group) and were administered intravenously via the tail with (Group 1) saline (100 µL), (Group 2) saline (100 µL) + NIR laser, (Group 3) RV (100 μ L, 3.6 mg kg⁻¹), (Group 4) MoS₂ (100 μ L, 2 mg kg⁻¹) + NIR laser, (Group 5) MoS₂-RV and (Group 6) MoS₂-RV (100 µL, in term of 3.6 mg kg⁻¹ RV and 2 mg kg⁻¹ MoS₂) + NIR laser. The NIR laser (1 W cm⁻², 5 min) was used for irradiation at 24 h post-injection of various samples. During the treatment, the relative tumor volume $(V/V_0, V_0$ represented the tumor volume when the tumor treatment was initiated) and mice body weight were monitored every three days. In addition, the tumors of the corresponding mice after 0, 7 and 21 days of treatment were excised for digital imaging. Major organs (heart, liver, spleen, lung, and kidney) of those mice were collected, fixed in 4% formalin, paraffin embedded into sections, and stained with hematoxylin and eosin (H&E). The images of these stained sections were captured with a digital camera.

Results and discussion

Preparation and characterization of MoS₂ nanosheets

Fig. 1 illustrates schematically the preparation of MoS_2 nanosheets from bulk MoS_2 and the NIR-triggered delivery of drugs for tumor therapy. In brief, the commercial bulk MoS_2 was first sonicated in an ice-bath using tip sonication for 2 h, and then the BSA powder was added into the mixture followed by sonication using a sonic bath with a low energy density for 10 h. Finally, the hybrid was centrifuged, and the supernatant was collected to obtain the purified MoS_2 nanosheets.

We studied the morphology of MoS₂ using atomic force microscopy (AFM) and found that the thickness of the asprepared MoS₂ nanosheets (Fig. 2A and B) was 5–15 nm, while the thickness of bulk MoS₂ with slight ultrasonication was 40– 70 nm (Fig. 2C and D). On the basis of the following two reasons, we can infer that the MoS₂ nanosheets are few layered nanosheets: (i) the thickness of non-functionalized single-layer MoS₂ nanosheets is mostly reported as 0.8–1.0 nm, and (ii) BSA molecules attach on both planes of MoS₂ nanosheets.^{19,26,30} The TEM images further confirmed the sheet structure of MoS₂ nanosheets (Fig. 2E) with an ultra-high surface area. As shown in Fig. 2F, the size distribution of MoS₂ nanosheets is in the range of 40–150 nm, while the average diameter is about 89 nm. Additionally, as evident in Fig. 3A and B, compared with the absorption spectrum of bulk MoS₂, the absorption spectrum of the MoS₂ nanosheets shows a new peak at 275 nm originating from BSA (Fig. 3C); the other two new peaks at 608 nm and 668 nm and about a 7-fold enhanced NIR absorbance further confirm the formation of few layered and ultra-small MoS₂ nanosheets.18 MoS2 nanosheets exhibited a well-dispersed state in water over one month (Fig. 3B inset), probably due to the adhesion of BSA on the MoS₂ nanosheet surface, while the bulk MoS₂ had serious aggregation under the same condition (Fig. 3B inset). Moreover, as shown by the thermogravimetric analysis (TGA) of MoS₂ nanosheets in Fig. 3D, a weight loss of 34.5%, which may be attributed to the absorption of BSA, was calculated within the temperature range of 100-400 °C,19 further demonstrating the existence of BSA adherence on MoS₂ nanosheets. Here, BSA, not only acts as an auxiliary agent of ultrasonic exfoliation, but also functions as a surfactant for MoS₂ nanosheets.

Preparation and characterization of MoS₂-RV

Similar to graphene, MoS_2 nanosheets are 2D material with an ultra-high surface area, therefore, MoS_2 may also be exploited as a carrier for delivering various functional molecules through non-covalent interactions such as π - π stacking and

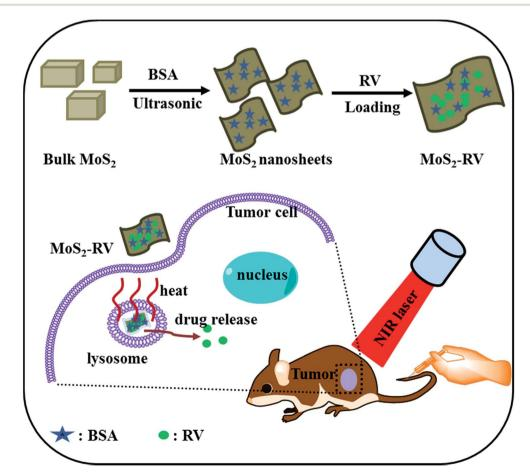


Fig. 1 A schematic representation of MoS₂ nanosheet synthesis and its photothermal-triggered drug delivery application.

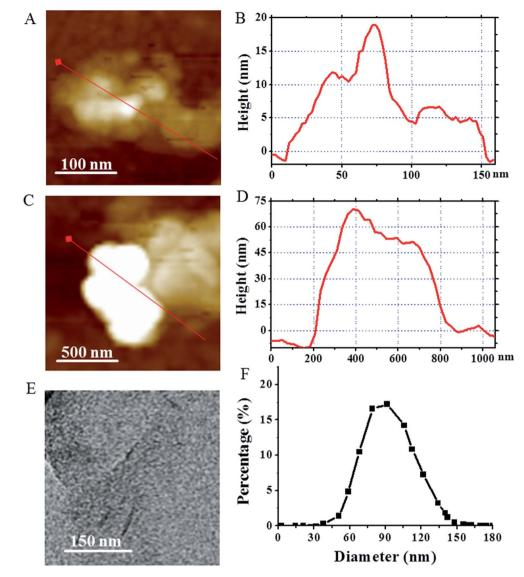


Fig. 2 (A and C) The AFM images of MoS_2 nanosheets (A) and bulk MoS_2 (C), respectively. (B–D) The corresponding AFM height analysis for MoS_2 nanosheets (B) and bulk MoS_2 (D), respectively. (E) The TEM image of MoS_2 nanosheets. (F) The size distribution of MoS_2 nanosheets as measured by DLS.

hydrophobic interactions.^{25,31} Resveratrol (RV), a phytoalexin found in grapes and other food products, has been known to have a cancer chemopreventive and chemotherapeutic effect on many tumors.³² In this study, we non-covalently loaded RV onto MoS₂ nanosheets by simply mixing the RV and MoS₂ at pH = 7.4. After removal of unbound RV by repeated filtration and centrifugation, we characterized the purified MoS₂–RV using UV-vis spectrophotometry. In Fig. 4A, the absorption spectrum of the MoS₂–RV shows both the feature peaks, corresponding to RV (306 nm) and BSA (275 nm), indicating the successful loading of RV onto MoS₂ nanosheets. Moreover, we observed significant RV fluorescence quenching after loading onto MoS₂ nanosheets (Fig. S1†), indicating further the strong interactions between MoS₂ nanosheets and RV molecules.

Fig. 4B shows that the RV loading capacities on MoS₂ nanosheets increases with increasing drug concentrations. The

highest RV loading ratios (weight ratios between the drug and MoS_2 nanosheets) at our tested conditions were determined to be ~180%, and the RV loading efficiency (the percentage of loaded RV in MoS_2 -RV) was ~65.8%. In addition, the enhanced average diameter of MoS_2 -RV (125 nm) compared with that of MoS_2 nanosheets (Fig. S2†) further confirmed the binding of RV on MoS_2 nanosheets. The high RV loading ratio may result from the ultra-high surface area of the MoS_2 nanosheets.

 MoS_2 nanosheets exhibited stronger NIR absorbance intensity compared with that of bulk MoS_2 , thus making MoS_2 nanosheets a potential NIR photothermal agent. To investigate the photothermal effects, water and the aqueous solutions of bulk MoS_2 and MoS_2 nanosheets with the same concentration of Mo were exposed to an 808 nm NIR laser (1 W cm⁻², 5 min). As shown in Fig. 4C, after 5 min NIR irradiation, MoS_2 nanosheets (0.2 mg mL⁻¹) show a higher temperature increase (68

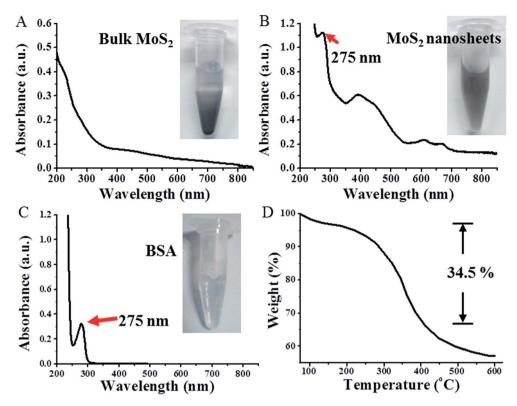


Fig. 3 The absorption spectra of bulk MoS₂ (A), MoS₂ nanosheets (B) and BSA (C), respectively. Insets are the corresponding images of bulk MoS₂ (A), MoS₂ nanosheets (B) and BSA (C) in aqueous solution, respectively. (D) TGA curve of MoS₂ nanosheets.

 $^{\circ}$ C) than bulk MoS₂ (38.5 $^{\circ}$ C), while pure water shows a small temperature change. The strong photothermal performance of MoS₂ nanosheets thus makes it a promising photothermal agent for tumor PTT therapy.

Fig. 4D shows that without laser irradiation, a maximum of 16.4% RV is released at pH 7.4 and a maximum of 39.5% RV is released at pH 5.0 from MoS₂ nanosheets within 48 h. Meanwhile, at the same condition, *i.e.*, at pH 5.0, we found that the RV release was sharply increased from 28.4% to 37.8% when MoS_2 -RV was irradiated for 5 min (1 W cm⁻²), whereas only 1.9% of RV was released during the subsequent 6 h of incubation without NIR irradiation. After five cycles of 5 min irradiation at 18 h, 30 h, 36 h, 42 h, and 48 h, respectively, the accumulated release of RV approached 50% after 48 h-much higher than that of RV released at pH 5.0 only. The results not only show that the pH value can induce the RV release, but also suggest that the NIR-light-induced local hyperthermia can function as a stimulus for the on-off control for RV release from the MoS₂ nanosheet surface. The RV release enhanced by NIR irradiation was deduced by the heat generated from MoS₂ nanosheets when absorbing the NIR light which induced more RV molecule release from MoS₂ nanosheets through weakening the non-covalent adsorption interaction between RV and MoS₂ nanosheets surface.33

Stability is a prime factor to be considered when developing nanomaterial for biomedical applications. As shown in Fig. 5A, after one month of storage at 4 °C, no apparent change is visible in the average diameters of MoS₂ and MoS₂–RV in water, indicating good stability. Moreover, Fig. 5B shows that 60 min of NIR irradiation (1 W cm^{-2}) does not change the RV characteristic peak (306 nm).³⁴

In vitro cell uptake

To evaluate the cellular uptake of MoS₂ nanosheets labeled by FITC,³⁵ we monitored the uptake using fluorescence microscopy. Raji cells cultured in six-well plates were incubated with free FITC and MoS₂/FITC at the same concentration of FITC for 4 h, respectively. The nucleus was then stained by DAPI. Fig. 6A shows much stronger green FITC fluorescence emitting from inside the cytoplasm in MoS₂/FITC treated cells, while less FITC fluorescence was seen in free FITC treated cells. The cellular uptake ratio of MoS₂/FITC detected by FCM was about 58.2%, while it was only 3.9% for that of free FITC (Fig. 6B), indicating that MoS₂ nanosheets could easily enter Raji cells and densely accumulate inside the cells.

Cytotoxicity and in vitro tumor therapy

Fig. 7A shows no obvious cytotoxicity of MOS_2 nanosheets for Raji cells even at high concentrations up to 200 µg mL⁻¹, while, after irradiating with the NIR laser for 5 min, the cell viability shows an obvious dose-independent decrease, indicating good biocompatibility and photothermal cytotoxicity of MOS_2 nanosheets. In addition, Fig. S3† showed that MOS_2 nanosheets and MOS_2 -RV had no obvious toxicity on bone marrow cells. To further investigate the therapeutic efficacy of the NIR

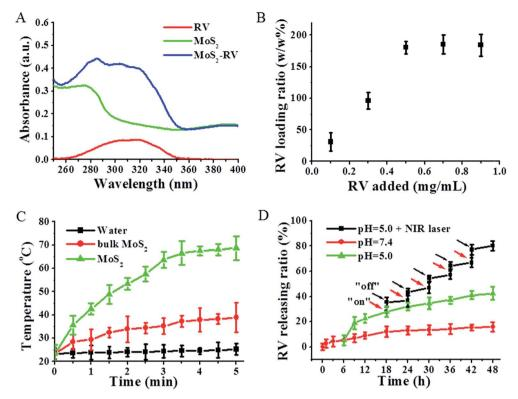


Fig. 4 (A) The absorption spectra of RV, MoS_2 nanosheets and MoS_2 -RV, respectively. (B) RV loading ratio onto MoS_2 nanosheets as a function of added RV concentrations. (C) Temperature increase of water and MoS_2 samples as a function of irradiation time. (D) Release kinetics of RV from MoS_2 nanosheets in PBS buffer (pH = 7.4 and 5.0) and in PBS buffer (pH = 5.0) in the absence and presence of 808 nm NIR laser irradiation. The data are shown as mean \pm S.D. (n = 4).

photothermal-triggered drug delivery system, we treated Raji cells with RV and MoS_2 -RV at the same RV concentration for 24 h with or without NIR laser irradiation. According to Fig. 7B, MoS_2 -RV with NIR laser irradiation (1 W cm⁻², 808 nm) for 5 min exhibits a higher cell-killing effect in Raji cells at all tested concentrations when compared with the RV, RV + NIR laser, MoS_2 -RV, and MoS_2 + NIR laser treated group alone. These findings suggest a significant synergistic cell-killing effect of MoS_2 -RV under the NIR laser irradiation, which could be

attributed to the combination of hyperthermia of MoS₂ nanosheets with chemotherapy. Moreover, the hyperthermia of MoS₂ can effectively enhance the delivery and release ratio of RV into cells, thus increasing the anti-cancer effect on Raji cells *in vitro*.

In vivo biodistribution and tumor therapy

Fig. 8A shows the biodistribution of MoS_2 in major tissues (including heart, liver, spleen, lung, kidney, and tumor) after 3 h, 1 day, 3 days, 5 days and 7 days intravenous administration of

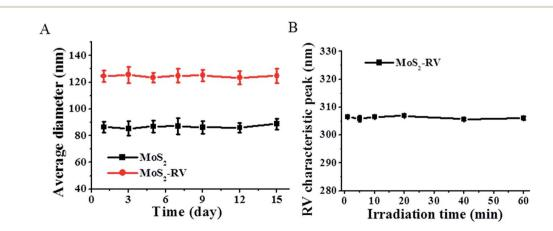


Fig. 5 (A) The average diameter changes of MoS_2 nanosheets and MoS_2 -RV, respectively in PBS buffer over 15 days. (B) The RV characteristic peak change of MoS_2 -RV under 808 nm laser irradiation (1 W cm⁻²) for different times. The data are shown as mean \pm S.D. (n = 4).

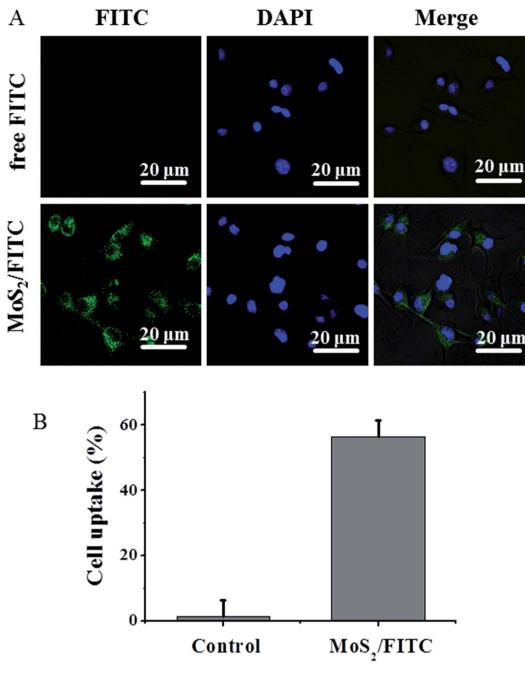


Fig. 6 (A) Confocal fluorescence images of Raji cells after incubation with free FITC and MoS₂/FITC. Green and blue colors represent FITC fluorescence and DAPI stained cell nuclei, respectively. (B) Flow cytometry measurement of cellular FITC fluorescence intensities in Raji cells after incubation with free FITC and MoS₂/FITC.

 MoS_2 -RV. We found that the maximum amounts of Mo elements were accumulated in the liver, spleen, and tumor within the first 24 h. However, after 24 h, the Mo content in these tissues decreased gradually with time, implying that the MoS_2 nanosheets could be excreted out of these organs, thus avoiding the potential adverse effects. The high accumulation of MoS_2 -RV in tumors may be ascribed to the enhanced permeation and retention (EPR) effect of a solid tumor and the fact that BSA absorbed on MoS_2 can improve the hemocompatibility and blood circulation durations.³⁶ Encouraged by the highly synergistic anti-cancer efficiency *in vitro* and tumor passive targeting effect, we further conducted *in vivo* tumor therapy on Raji tumor-bearing mice. After administering different samples through intravenous tail injection and comparing with the control groups treated by saline and saline + NIR laser, the mice treated by RV, MoS₂ + NIR laser and MoS₂–RV alone lowered the tumor growth rate, but did not exhibit complete tumor suppression. As expected, the MoS₂–RV + NIR laser showed a significantly suppressed tumor growth and no relapse after the treatment (Fig. 8B), consistent with the tumor appearance of the

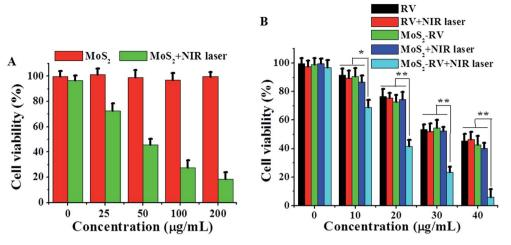


Fig. 7 (A) Cell viabilities of Raji cells after incubation with different concentrations of MoS_2 nanosheets with or without 808 nm laser irradiation (1 W cm⁻²) for 5 min. (B) Cell viabilities of Raji cells after incubation with different concentrations of RV and MoS_2 -RV with or without 808 nm laser irradiation (1 W cm⁻²) for 5 min. The data are shown as mean \pm S.D. (n = 4). *p < 0.05, **p < 0.01.

tumor bearing mice after 0, 7 and 21 days of treatment (Fig. S4†). Therefore, we can infer that compared with the monotherapy, MoS_2 -RV combined photothermal therapy exhibits a higher

synergistic anti-cancer effect on the tumor cells probably due to the photothermal enhanced drug delivery and the high tumor accumulation of MoS_2 -RV.

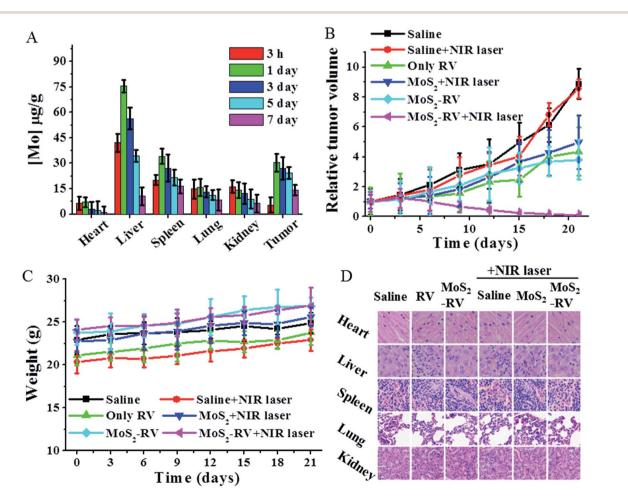


Fig. 8 (A) Biodistribution of Mo in the major organs, including the heart, liver, spleen, lung, kidney, and tumor at different time points posttreatment with MoS_2 -RV. (B) The growth profile of Raji xenografted tumors after various treatments as indicted. NIR laser was irradiated for 5 min, 24 h post-injection. (C) Body weight of Raji tumor-bearing mice after various treatments as indicted. (D) H&E-stained tissue sections of major organs, including the heart, liver, spleen, lung, and kidney, from the mice after treatments as indicated (magnification: 200×).

Furthermore, we monitored the body weights of mice in different groups and found no obvious weight variation over time when compared with the saline treated mice (Fig. 8C). The *in vivo* systemic toxicity was further evaluated by H&E staining of the major organs including the heart, liver, spleen, lung, and kidney after three weeks of treatments (Fig. 8D). No noticeable tissue toxicity or abnormality was found from the corresponding tissue H&E stained images in all tested groups. Moreover, Table S1[†] showed that MoS₂ nanosheets and MoS₂–RV had no significant influence on mice peripheral blood cells including white blood cells, red blood cells and platelets through the blood cell count method. These results further guaranteed the *in vivo* safety of MoS₂–RV for biomedical applications.

Conclusions

In summary, the MoS₂ nanosheets prepared by a facile method have great potential as an ideal photothermal-triggered drug delivery nanoplatform for synergistic tumor therapy. The as-made MoS₂ nanosheets not only exhibited high stability in aqueous media and great biocompatibility, they also showed 7-fold enhanced NIR absorbance in comparison with bulk MoS₂, thus inducing a high photothermal effect. MoS₂ nanosheets exhibited high RV loading capacity *via* non-covalent interaction. Most importantly, MoS₂–RV exhibited a controllable drug release response to NIR laser irradiation and pH value. Furthermore, the MoS₂–RV coupled with NIR-mediated hyperthermia and heatinduced local drug release demonstrated outstanding synergistic cell-killing and tumor growth suppression effect both *in vitro* and *in vivo* without any toxicity to the healthy tissues.

Conflict of interest

The author reports no conflicts of interest in this work.

Notes and references

- 1 T. Lammers, S. Aime, W. E. Hennink, G. Storm and F. Kiessling, *Acc. Chem. Res.*, 2011, **44**, 1029–1038.
- 2 R. Bardhan, S. Lal, A. Joshi and N. J. Halas, *Acc. Chem. Res.*, 2011, 44, 936–946.
- 3 F. M. Kievit and M. Zhang, Acc. Chem. Res., 2011, 44, 853-862.
- 4 Y. Liu, K. Ai, J. Liu, M. Deng, Y. He and L. Lu, *Adv. Mater.*, 2013, **25**, 1353–1359.
- 5 K. Yang, L. Hu, X. Ma, S. Ye, L. Cheng, X. Shi, C. Li, Y. Li and Z. Liu, *Adv. Mater.*, 2012, **24**, 1868–1872.
- 6 L. Cheng, K. Yang, Q. Chen and Z. Liu, *ACS Nano*, 2012, 6, 5605–5613.
- 7 Z. Zha, S. Zhang, Z. Deng, Y. Li, C. Li and Z. Dai, *Chem. Commun.*, 2013, **49**, 3455–3457.
- 8 M. F. Tsai, S. H. Chang, F. Y. Cheng, V. Shanmugam, Y. S. Cheng, C. H. Su and C. S. Yeh, *ACS Nano*, 2013, 7, 5330–5342.
- 9 A. Y. Lin, J. K. Young, A. V. Nixon and R. A. Drezek, *Small*, 2014, **10**, 3246–3251.
- 10 M. Chen, S. Tang, Z. Guo, X. Wang, S. Mo, X. Huang, G. Liu and N. Zheng, *Adv. Mater.*, 2014, **26**, 8210–8216.

- 11 X. Song, Q. Chen and Z. Liu, Nano Res., 2015, 8, 340-354.
- 12 S. M. Sharker, J. E. Lee, S. H. Kim, H. J. Ji, I. In, H. Lee and S. Y. Park, *Biomaterials*, 2015, **61**, 229–238.
- 13 P. R. Jheng, K. Y. Lu, S. H. Yu and F. L. Mi, *Colloids Surf.*, *B*, 2015, **136**, 402-412.
- 14 C. Zhang, T. Lu, J. Tao, G. Wan and H. Zhao, *RSC Adv.*, 2016, 6, 15460–15468.
- 15 R. Lv, J. A. Robinson, R. E. Schaak, D. Sun, Y. Sun, T. E. Mallouk and M. Terrones, *Acc. Chem. Res.*, 2014, 48, 56–64.
- 16 L. Kangho, G. Riley, M. E. Niall, H. Toby and G. S. Duesberg, *Adv. Mater.*, 2013, **25**, 6699–6702.
- 17 A. Splendiani, L. Sun, Y. Zhang, T. Li, J. Kim, C. Y. Chim, G. Galli and F. Wang, *Nano Lett.*, 2010, 10, 1271–1275.
- 18 D. Gopalakrishnan, D. Damien and M. M. Shaijumon, ACS Nano, 2014, 8, 5297–5303.
- 19 G. Guan, S. Zhang, S. Liu, Y. Cai, M. Low, C. P. Teng, I. Y. Phang, Y. Cheng, K. L. Duei, B. M. Srinivasan, Y. Zheng, Y. W. Zhang and M. Y. Han, *J. Am. Chem. Soc.*, 2015, 137, 6152–6155.
- 20 S. Wang, X. Li, Y. Chen, X. Cai, H. Yao, W. Gao, Y. Zheng, X. An, J. Shi and H. Chen, *Adv. Mater.*, 2015, 27, 2775–2782.
- 21 S. Wang, K. Li, Y. Chen, H. Chen, M. Ma, J. Feng, Q. Zhao and J. Shi, *Biomaterials*, 2015, **39**, 206–217.
- 22 X. Li, Y. Gong, X. Zhou, H. Jin, H. Yan, S. Wang and J. Liu, *Int. J. Nanomed.*, 2016, **11**, 1819–1833.
- 23 S. Wang, Y. Chen, X. Li, W. Gao, L. Zhang, J. Liu, Y. Zheng,
 H. Chen and J. Shi, *Adv. Mater.*, 2015, 27, 7117–7122.
- 24 X. Wang, Q. Zhang, L. Zou, H. Hu, M. Zhang and J. Dai, *RSC Adv.*, 2016, **6**, 20949–20960.
- 25 T. Liu, C. Wang, X. Gu, H. Gong, L. Cheng, X. Shi, L. Feng,
 B. Sun and Z. Liu, *Adv. Mater.*, 2014, 26, 3433–3440.
- 26 W. Yin, L. Yan, J. Yu, G. Tian, L. Zhou, X. Zheng, X. Zhang, Y. Yong, J. Li, Z. Gu and Y. Zhao, ACS Nano, 2014, 8, 6922– 6933.
- 27 J. K. Aluyen, Q. N. Ton, T. Tran, A. E. Yang, H. B. Gottlieb and R. A. Bellanger, *J. Diet. Suppl.*, 2012, 9, 45–56.
- 28 Q. Ji, X. Liu, X. Fu, L. Zhang, H. Sui, L. Zhou, J. Sun, J. Cai, J. Qin, J. Ren and Q. Li, *PLoS One*, 2013, 8, e78700.
- 29 M. Swamydas and M. S. Lionakis, J. Visualized Exp., 2013, e50586.
- 30 T. Liu, C. Wang, W. Cui, H. Gong, C. Liang, X. Shi, Z. Li,
 B. Sun and Z. Liu, *Nanoscale*, 2014, 6, 11219–11225.
- 31 M. Nurunnabi, K. Parvez, M. Nafiujjaman, V. Revuri, H. A. Khan, X. Feng and Y. Lee, *RSC Adv.*, 2015, 5, 42141– 42161.
- 32 T. Yang, L. Wang, M. Zhu, L. Zhang and L. Yan, *Pharmazie*, 2015, **70**, 501–506.
- 33 W. Fang, S. Tang, P. Liu, X. Fang, J. Gong and N. Zheng, Small, 2012, 8, 3816–3822.
- 34 K. P. L. Bhat, J. W. Kosmeder and J. M. Pezzuto, *Antioxid. Redox Signaling*, 2001, **3**, 1041–1064.
- 35 Z. Huang, Y. Qi, D. Yu and J. Zhan, *RSC Adv.*, 2016, **6**, 31031–31036.
- 36 H. Maeda, H. Nakamura and J. Fang, *Adv. Drug Delivery Rev.*, 2013, **65**, 71–79.